

STRUCTURAL DEFECTS AND THEIR RELATIONSHIP TO NUCLEATION OF GaN THIN FILMS

WEIDA QIAN*, MAREK SKOWRONSKI, AND GREG S. ROHRER
Department of Materials Science & Engineering
Carnegie Mellon University, Pittsburgh, PA 15213

*current address: Department of Materials Science, Northwestern University, Evanston, IL 60208

ABSTRACT

Microstructure and extended defects in α -GaN films grown by organometallic vapor phase epitaxy on sapphire substrates using low temperature AlN (or GaN) buffer layers have been studied using transmission electron microscopy. The types and distribution of extended defects were correlated with the film growth mode and the layer nucleation mechanism which was characterized by scanning force microscopy. The nature of the extended defects was directly related to the initial three-dimensional growth. It was found that inhomogeneous nucleation leads to a grain-like structure in the buffer; the GaN films then have a columnar structure with a high density of straight edge dislocations at grain boundaries which are less likely to be suppressed by common annihilation mechanisms. Layer-by-layer growth proceeds in many individual islands which is evidenced by the observation of hexagonal growth hillocks. Each growth hillock has an open-core screw dislocation at its center which emits monolayer-height spiral steps.

INTRODUCTION

Gallium nitride and its related alloys (AlGaN and InGaN) are important wide band-gap semiconductors that have potential applications in both short wavelength optoelectronic and high power/high frequency devices [1-4]. Epitaxial films of GaN have been grown by organometallic vapor phase epitaxy (OMVPE) [5] and molecular beam epitaxy (MBE) [6,7], on a number of substrates including Si [8,9], GaAs [10], SiC[11], α -Al₂O₃ (sapphire) [12,13] and MgO [14]. Among them, sapphire is the most common substrate and generally yields the best film. However, nitride films deposited on sapphire, which is poorly matched to GaN both in terms of lattice parameter and thermal expansion coefficient (see Table I), are known to contain a high density of extended defects (mainly threading dislocations) [15,16]. These defects affect both the electrical and optical properties of the material and are known to be detrimental to its device applications. For example, dislocation cores can form non-radiative recombination centers which limit the efficiency of light emitting diodes and often lead to injection failures in lasers. By low temperature deposition of an AlN (or GaN) buffer layer, the crystal quality of the GaN epilayers can be considerably improved [13,17]. However, such films typically have dislocation densities in the 10^9 - 10^{10} cm⁻² range [15,16].

It is widely accepted that the crystal structure, the nature and relative concentration of extended defects in group-III nitride films are strongly influenced by the growth techniques and conditions used, and by the type and orientation of the substrates. The dominant defects in OMVPE grown GaN films on sapphire are straight threading dislocations which penetrate the entire GaN film [16]. Both the structural and electron optical properties of the GaN film depends on the thickness, the deposition temperature of the low temperature buffer, and the orientation of the sapphire substrate [18-20]. In this paper, we report studies of OMVPE growth of GaN on sapphire using a low temperature AlN (or GaN) buffer layer, with particular emphasis on its initial nucleation and its relation to the resulting microstructure. GaN films grown on either (0001) (c plane) or (11 $\bar{2}$ 0) (a plane) sapphire substrates under different conditions were studied by transmission electron microscopy (TEM). The types and distribution of extended defects were correlated with the film

growth mode and the layer nucleation mechanism which was characterized by scanning force microscopy.

Table I. Lattice parameters (in Å) and thermal expansion coefficients (in K⁻¹) of wurtzite GaN, AlN and hexagonal α-Al₂O₃

		GaN	AlN	α-Al ₂ O ₃
Lattice parameter	a	3.189	3.111	4.758
	c	5.178	4.979	12.991
Thermal exp. coefficient	a	5.59×10 ⁻⁶	4.2×10 ⁻⁶	7.5×10 ⁻⁶
	c	3.17×10 ⁻⁶	5.3×10 ⁻⁶	8.5×10 ⁻⁶

EXPERIMENTAL

The GaN samples used in this study were grown on both (0001) and (11 $\bar{2}$ 0) sapphire substrates using an inductively-heated, water cooled, vertical OMVPE reactor operated at 57 torr [19,20]. An AlN (or GaN) buffer layer, 200 to 500 Å in thickness, was deposited at 450 °C to 550 °C before the high temperature deposition of GaN. TEM specimens were prepared by first lapping with diamond paste on a titanium plate down to a thickness of about 100 μm, followed by polishing with consecutively smaller size diamond pastes and/or alumina (Al₂O₃) in a Gatan dimpler down to a thickness of about 20 μm. The specimen was then sputtered to electron transparency by Ar⁺ at liquid nitrogen temperature. Transmission electron microscopy observations were carried out on a Philips EM420-TEM and a JEOL 4000 EX-TEM, operated at 120 keV and 400 keV, respectively. For surface observations, the as-grown films were examined in air with a Park Scientific Instruments scanning force microscope. The 5 μm scanner was operated at 2 Hz. All images were acquired in the constant force mode using 3 to 12 nN of contact force.

RESULTS

Crystalline Orientation and the Interface

GaN epitaxial layers grown on both c-plane and a-plane α-Al₂O₃ substrates crystallize with the wurtzite structure and the growth is along the c-axis. The crystal orientation relationships of GaN and AlN grown on sapphire substrates are summarized in Table II. Selected area electron diffraction (SAD) and high resolution electron microscopy reveal that both GaN and AlN layers grow epitaxially on their substrates. For growth on (0001) α-Al₂O₃, the epitaxial relationships were determined to be: (0001)_{GaN}//(0001)_{AlN}//(0001)_{α-Al₂O₃}, with in-plane orientation relations of [1 $\bar{1}$ 00]_{GaN}//[1 $\bar{1}$ 00]_{AlN}//[11 $\bar{2}$ 0]_{α-Al₂O₃}, in agreement with previously published results [15, 21]. For growth on (11 $\bar{2}$ 0) α-Al₂O₃, both GaN (0001) and AlN (0001) planes were found to be parallel to the (11 $\bar{2}$ 0) substrate plane, with in-plane orientation relations of [1 $\bar{1}$ 00]_{GaN}//[1 $\bar{1}$ 00]_{AlN}//[0001]_{α-Al₂O₃}, in accordance with observations by other groups [12, 22,23].

Table II. Epitaxial relationships during growth of GaN, AlN on c- and a-plane sapphire

Growth direction		In-plane orientation relationship	
Epilayer	Substrate	Epilayer	Substrate
(0001)GaN (0001)AlN	(0001) α -Al ₂ O ₃	[1 $\bar{1}$ 00] GaN [1 $\bar{1}$ 00] AlN	[11 $\bar{2}$ 0] α -Al ₂ O ₃
(0001) GaN (0001) AlN	(11 $\bar{2}$ 0) α -Al ₂ O ₃	[1 $\bar{1}$ 00] GaN [1 $\bar{1}$ 00] AlN	[0001] α -Al ₂ O ₃

The interface between the AlN (or GaN) buffer layer and the sapphire substrate was found to be locally coherent and the misfit dislocation spacing is almost uniform. Figure 1 shows the TEM micrographs of the AlN/(0001) α -Al₂O₃ interface. The measured misfit dislocation spacing shown in figure 1a is 2.1 nm, which is close to the expected spacing of 2.2 nm corresponding to a fully relaxed layer (about 14 % lattice constant mismatch between AlN and sapphire). Similar

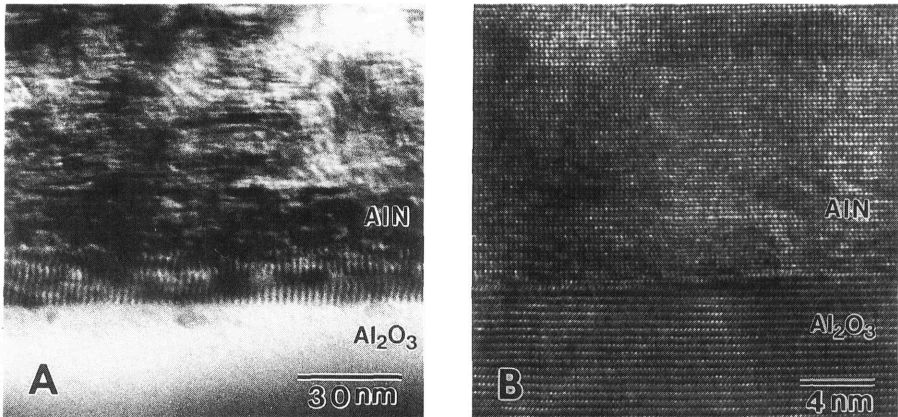


Figure 1. Transmission electron micrographs of the AlN/(0001) α -Al₂O₃ interface: (a). bright field image shows misfit dislocations at the AlN/sapphire interface; (b). Lattice image along [1 $\bar{1}$ 00] of sapphire shows the crystalline structure.

results have been reported during AlGaN epitaxial growth on sapphire [24]. The high resolution TEM micrograph shown in figure 1b reveals that the interface of AlN/(0001) α -Al₂O₃ is sharp, with the {1 $\bar{1}$ 00} planes of AlN parallel to the {11 $\bar{2}$ 0} planes of sapphire and the basal (0002) planes of AlN parallel to those of sapphire. Surface steps on the sapphire side are most likely due to the interaction of ammonia (NH₃) during surface treatments before deposition. However, extensive observation along the interface with high resolution TEM reveals that, along with many

extended defects, the AlN buffer layer is typically composed of columnar fine crystals [21]. Lateral dimension of columnar grains is on the order of 10 nm, and the misorientation among neighboring grains is a few degrees. The GaN/sapphire interface and the GaN buffer layer exhibits similar features. The columnar structures were also reported in GaN films grown on 6H SiC [25].

Microstructure and the Extended Defects

Figure 2a shows the cross-sectional weak beam TEM micrograph of a GaN film grown on (11 $\bar{2}$ 0) α -Al $_2$ O $_3$ using a 375 Å GaN buffer layer deposited at 450 °C, imaged near the [1 $\bar{1}$ 00] orientation with the active beam of $g=11\bar{2}0$. The dominant defects in the GaN film are dislocations resulting from the misfit strain introduced by the lattice mismatch between the epilayer and the substrate, and low angle grain boundaries. A high density of dislocation half loops and stacking faults along {0002} GaN planes were observed in regions close to the buffer. A defect density reduction of about an order of magnitude was observed within the initial 0.4 μ m of the GaN film. In the immediate vicinity of the low temperature buffer layer, the defect density was so high that we were unable to resolve the defects individually using conventional TEM. At small film thickness, the dislocation lines in the GaN epilayer orient themselves irregularly. However, at film thickness larger than about 0.6 μ m, most remaining threading dislocations lie close to the [0001] growth direction [16].

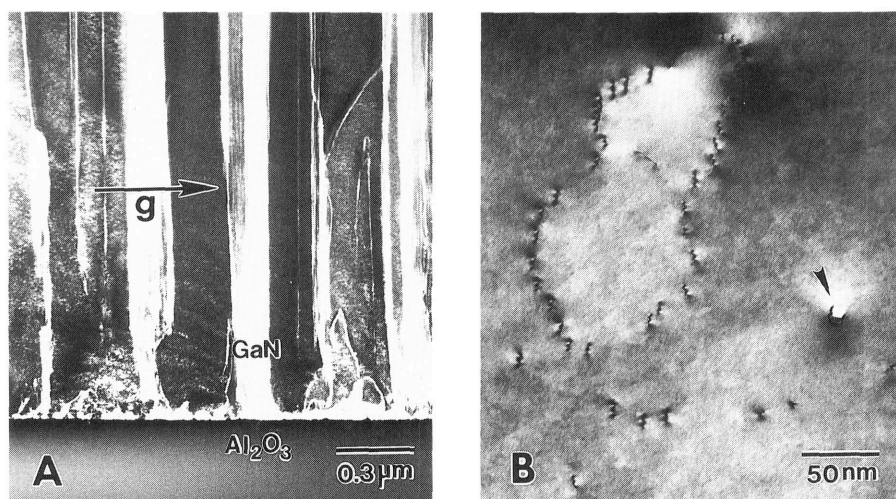


Figure 2. TEM micrographs of a GaN film grown on a-plane sapphire with a 375 Å GaN buffer layer deposited at 450 °C. (a). Weak beam cross-sectional view; (b). Bright field plan-view.

When viewed from plan-view TEM micrographs (Fig. 2b), the extended defects in relatively thick (thicker than about 1 μ m) GaN films are basically of two types: threading dislocations and nanopipes (labeled with an arrow) [26]. The threading dislocation density near the top surface of a 3 μ m thick GaN layer is typically on the order of $10^9 \sim 10^{10}/\text{cm}^2$, as measured using plan-view TEM. It has been reported that other extended defects, such as microtwins and double-positioning

boundaries were frequently observed at the vicinity of the GaN/substrate interface using cross sectional high resolution TEM [9,25,27].

Threading Dislocations

A typical plan-view bright field TEM micrograph ($g=11\bar{2}0$) of an α -GaN film grown on sapphire is shown in Fig. 3a. Since the TEM specimen was polished only from the substrate side, Fig. 3a is representative of GaN films that are thicker than about 2 μm . Except for a relatively small density of nanopipes (not shown), the defects are almost exclusively threading dislocations. All the threading dislocation lines form short segments, indicating that they are lying close to the film growth direction (c-axis). The majority of them are pure edge, with Burgers vectors of the $1/3\langle 11\bar{2}0 \rangle$ type, and are arranged to form well defined low angle grain boundaries. The grain size ranges from 50 nm to 500 nm, while the dislocation spacing at the boundaries ranges from 5 to 50 nm, corresponding to in-plane misorientations of less than 3° [16]. Through TEM observations carried out on large number of MOVPE GaN films grown under different conditions, we found that low angle grain boundaries are the main source of threading dislocations. Threading density in the GaN film shown in figure 3b, which has less grain-like structure, is about one order of magnitude lower than that in the film which is shown in figure 3a ($10^9/\text{cm}^2$ compared to $10^{10}/\text{cm}^2$).

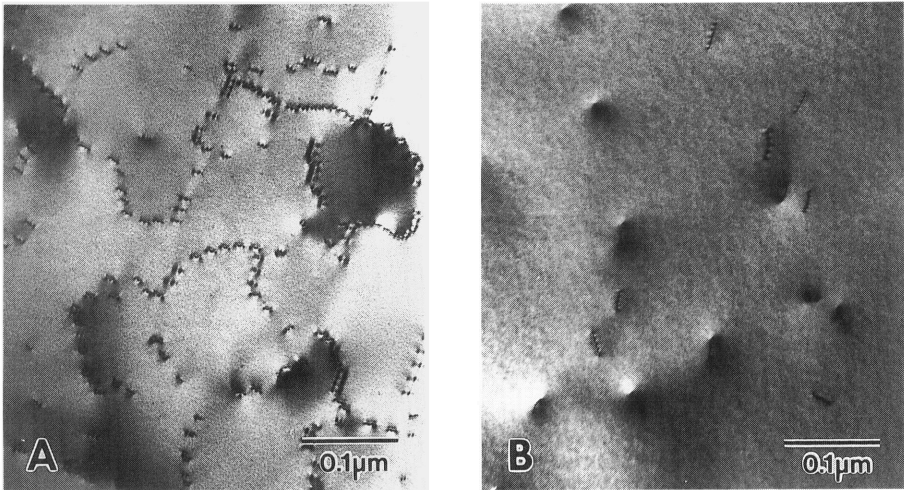


Figure 3. Plan-view TEM micrographs of GaN films grown on sapphire. (a). A typical micrograph taken from samples with high threading densities. The majority of threading dislocations form well defined low angle grain boundaries. (b). A typical micrograph taken from samples with low threading densities, which shows less grain-like structure.

The grain-like structure can also be clearly observed in weak beam cross-sectional TEM micrographs (figure 2a). The image contrast is produced by differing diffraction conditions in neighboring grains. Except near the vicinity of the buffer layer, the dimension of each grain keeps an almost constant value throughout the GaN film. The individual dislocations at grain boundaries

can hardly be resolved in thicker cross-sectional specimens since many of them overlap along the beam direction. Although high resolution TEM micrograph often reveals some local tilting of *c*-planes in some regions, grain misorientation along the *c*-axis is much smaller and could not be detected by electron diffraction experiments. In fact, x-ray rocking curves [(0004) reflection] taken from these samples have a typical width of 200 - 350 arcsecs [19,20].

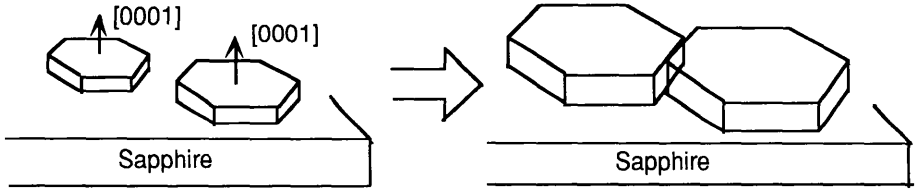


Figure 4. Schematic representation of the initial growth of GaN on sapphire and the formation of grain-like structures in the film.

Low angle grain boundaries are believed to be formed during coalescence of islands at the initial stages of GaN growth, based on the nucleation mechanism first proposed by Akasaki et al. [13]. The buffer layer is thought to have an amorphous-like structure at its deposition temperature (450 - 550 °C). It then recrystallizes and forms columnar fine crystals during annealing [21]. The initial growth of GaN is also highly three dimensional. Since these islands are more likely to preserve a hexagonal shape, and often have small misorientations with their neighbors, dislocation arrays are created during coalescence of these islands, as illustrated schematically in Fig. 4.

The reduction of the defect density within the initial 0.4 μm of the GaN film is most likely due to annihilation and coalescence through mutual interactions and the formation of half loops, as is evidenced in figure 2a. In these regions, both the defect density and the percentage of randomly oriented dislocations are high, and therefore, there is a high probability of defect interactions. However, the remaining quasi-parallel dislocations which thread along the growth direction are apparently not annihilated appreciably during further film growth because of their invariant mutual spacing along the growth direction.

It is well known that a strained layer superlattice (SLS) can be used to suppress threading dislocations in zinc-blende semiconductor epilayers [28]. The stress/strain field in the epilayer introduced by the SLS is used to initiate dislocation glide on the {111} slip planes, causing the dislocation lines to bend either towards another threading line so that they annihilate one another, or normal to the growth direction along the interface so that they do not propagate further into the epilayer. However, the threading dislocations in α-GaN films described above have slip planes of the {1 $\bar{1}$ 00} type, and generally require larger resolved shear stress to initiate glide. Furthermore, the stress/strain field introduced by the SLS is parallel to the (0001) growth plane, which does not provide driving force for dislocation glide on the {1 $\bar{1}$ 00} slip planes. Therefore, it can be expected that, to suppress, or eventually eliminate, this type of threading dislocations with a SLS could be more difficult. This argument is partially supported by our observations on several samples, each of which has a SLS composed of different periods of GaN/AlN layers placed at different positions in the GaN film. Figure 5 shows the cross-sectional TEM micrograph of a sample which has 5 periods of (6 nm GaN/6 nm AlN) placed after 2 μm of GaN film growth. An additional 0.5 μm GaN film was grown on top of the SLS. Although most dislocation lines were slightly bent as they passed through the SLS, only about 10% of threading dislocations were actually suppressed.

Basal plane dislocations were sometimes observed in regions far away from the buffer layer in a number of GaN films. Figure 6 shows a cross-sectional TEM micrograph taken from one of these samples. Detailed TEM analysis indicates that these are Frank partial loops containing stacking faults. Though more complete work is needed to develop a satisfactory explanation for the formation of these dislocations, an unstable growth condition or the thermal stresses [29] might be responsible for their formation.

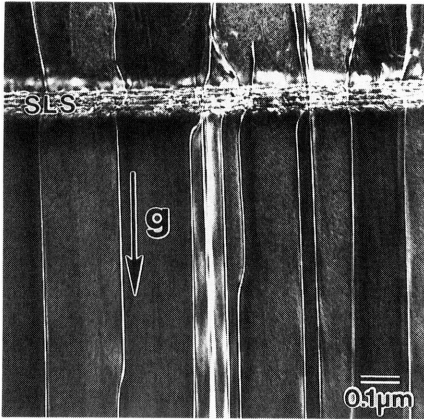


Figure 5. Cross-sectional TEM micro-graph showing the ineffectiveness of a SLS for threading dislocation suppression in the GaN films.

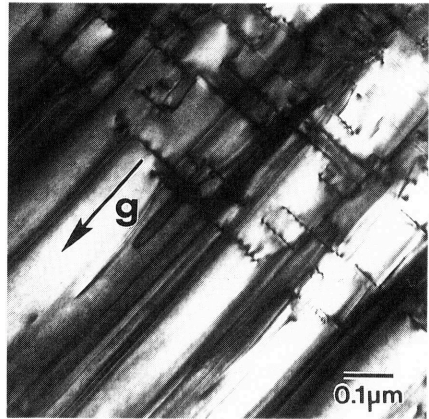


Figure 6. Cross-sectional TEM micro-graph showing GaN basal plane dislocations in regions near the inserted AlN thin layer.

Nanopipes

In addition to threading dislocations, another major type of extended defect in GaN films which is potentially detrimental to device applications is the nanopipes which has an estimated density of $10^5 - 10^7 / \text{cm}^2$. These defects are long, faceted empty tubes that penetrate through the GaN epilayer [26,30]. The radii of the pipes are in the 3 - 50 nm range and they appear to propagate along the c-axis of the film. Figure 7 shows plan-view bright field images of GaN film from a region containing a nanopipe (marked with letter A). In figure 7a, the micrograph was taken along the [0001] zone axis, in which the pipe is a perfect hexagon with a diameter of about 9 nm. Two dislocations (marked with letters B and C) are visible along this orientation. After the specimen was tilted about 30° until the (02 $\bar{2}$ 1) beam near the [1 $\bar{2}$ 16] zone axis was excited (figure 7b), a wavy contrast can be observed within the pipe which is similar to the contrast from dislocation lines, in addition to the contrast from the pipe walls. TEM analysis indicates that the nanopipe image contrast is in agreement with the **g**·**b** criteria for a screw dislocation of Burgers vector **b** = $n \times 1/3[0003]$ (where n is an integer and $c=5.18 \text{ \AA}$ for α -GaN). Figure 8 shows the lattice vector of a similar nanopipe taken with the [0001] orientation. The internal surfaces of the pipe are formed by six close-packed {1 $\bar{1}$ 00} prism planes (lattice spacing of 2.76 \AA), and a closed circuit drawn around the pipe shows no net atomic displacement. This was also the case for several other nanopipes examined in detail by HRTEM. Based on a combination of diffraction contrast analysis,

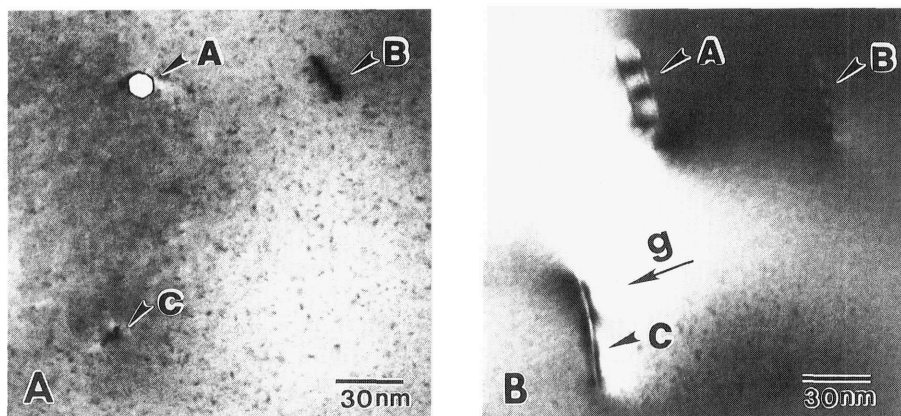


Figure 7. Bright field TEM micrographs of a nanopipe taken under different diffraction conditions. (a). Along the [0001] zone axis; (b). With $g=(02\bar{2}1)$.

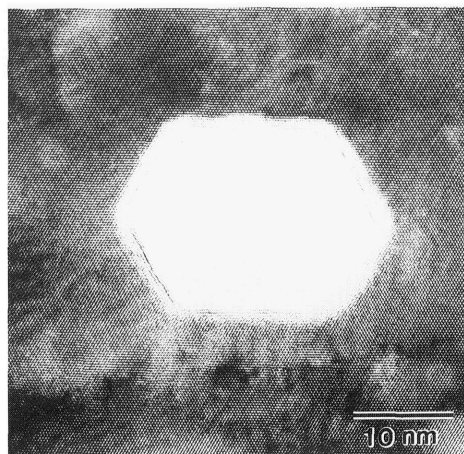


Figure 8. Lattice image of a nanopipe obtained with the [0001] zone axis. The internal surfaces of the pipe are formed by six close-packed $\{1\bar{1}00\}$ prism planes (lattice spacing of 2.76 Å).

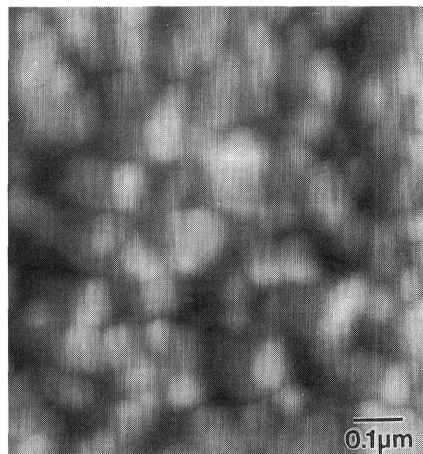


Figure 9. Scanning force microscopy image of a low temperature GaN buffer layer on c-plane $\alpha\text{-Al}_2\text{O}_3$. The buffer forms grain-like structure with surface roughness of about 20 nm, and the grain size of 100 nm.

high resolution TEM and scanning force microscopy (SFM) study (shown below), we conclude that these nanopipes are the open cores of screw dislocations with Burgers vectors of a single or multiple c parameters [26,30]. Another nanometer dimension defect along the growth direction has been reported in GaN films grown on sapphire, and has been characterized as microtwins due to local lattice twists or a difference in stoichiometry [23].

Similar, but orders of magnitude larger, open-core dislocations have been reported in a number of crystals including SiC [31,32] and some flux grown garnets [33]. The SiC micropipes have received the greatest attention because they are known to be the defects that limit the breakdown voltage of high power devices [34]. The Burgers vector associated with the spiral steps in SiC is usually greater than 100 Å and the defect is, therefore, visible in conventional optical microscopes.

The existence of open-core dislocations has been predicted by Frank [35], who argued that a state of local equilibrium exists in which a dislocation should have less energy when its core is hollow than when its core is filled with strained lattice. In other words, the open-core is the consequence of the balance between the surface free energy and the lattice strain energy in a dislocation. The lattice strain energy associated with a dislocation provides a driving force for preferential evaporation in the vicinity of the dislocation core [36]. For crystals with relatively large shear modulus and small surface free energy, an open-core should thus be established for dislocations with relatively large Burgers vectors. In fact, all the previously observed open-core dislocations have Burgers vector on the order of, or greater than, 10 Å. The smaller radii of the open-cores in GaN crystals by comparison to those previously observed in other crystals can be explained by its smaller lattice parameter ($c=5.2\text{Å}$). According to Frank's theory [35], the radius of the hole is proportional to the square of its Burgers vector. However, our observation do not quantitatively agree with Frank's theory [30].

GaN Surface and the Film Nucleation

Optical microscopy, scanning force microscopy (SFM) and scanning electron microscopy have been used to study the surface structure of the sapphire substrate, the buffer layer and the GaN free surface. Figure 9 shows a SFM image of a 100 nm thick low temperature GaN buffer layer deposited on c -plane $\alpha\text{-Al}_2\text{O}_3$. After annealing at 1025 °C, the buffer forms a grain-like structure with surface roughness of about 20 nm, and an island size of about 100 nm. However, our study revealed that surface morphology of the buffer layer is strongly influenced by its deposition and annealing temperatures, and by the substrate surface cleaning procedures. Lateral growth and smooth coalescence of islands could be promoted through carefully optimizing the buffer conditions. It has been recently reported that, before annealing, the low temperature GaN buffer layers consist of predominantly cubic phase with a high density of stacking faults and twins [37]. The average grain size increases with increasing layer thickness and annealing temperature. At temperatures necessary for the growth of high quality GaN (over 1000 °C), the buffer layer partially converts to hexagonal GaN [37].

The free surfaces of most GaN films typically exhibit cone-like and hexagonal mounds and ledge-facets that are only incompletely bounded by visible steps [38]. These mounds and ledge-facets, which have a typical dimension on the order of 10 μm and can be viewed under an optical microscope, are believed to be growth hillocks which are directly related to the three dimensional nature of the initial GaN growth. The ledge-facets are formed during coalescence of neighboring islands which have slight c -axis misorientations. These misorientations would result in increments in the x -ray rocking curve widths. The apparently large dimension of the growth hillocks compared to those of islands in the buffer can be explained by the mechanism proposed by Hiramatsu et al [21]. The initial growth of GaN is also columnar on top of the buffer fine crystals. During further growth, some fine crystals become larger size islands as the result of geometric selection [39]. The front area of each hillock increases as the merge continues, and the number of growth hillocks emerging at the front gradually decreases. However, there is no direct correlation between sizes of the growth hillocks and those of the small grains observed by TEM. The misoriented grains, bounded by arrays of edge dislocations, once formed, are not likely to expand.

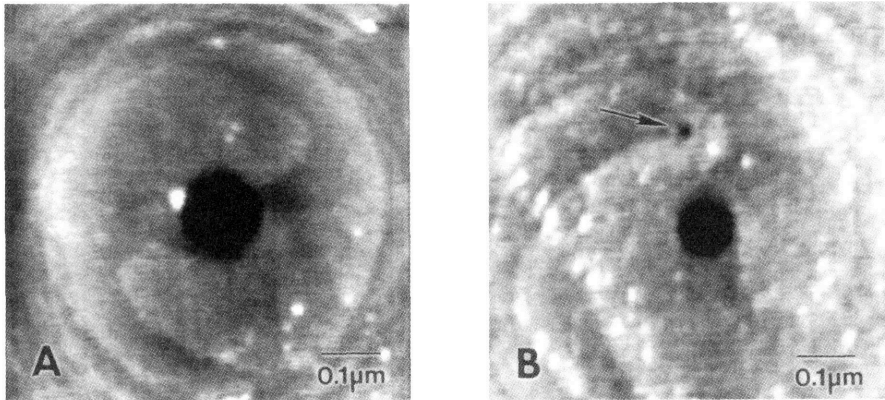


Figure 10. High resolution SFM images of open-core screw dislocations at the hillock centers. (a). A pair of monolayer spiral steps ($3.1 \pm 0.8 \text{ \AA}$) originate from the open core and propagate outwards; (b). A single spiral step in addition to a pair of monolayer spiral steps from the open core.

SFM observation reveals single atomic layer steps in flat regions between the hillocks and spiral single atomic layer steps on the top of faceted hillocks [30,37]. This indicates that at the later stages, GaN grows by both a layer-by-layer and a spiral mechanism [37]. Nanopipes were also observed during SFM observations [30,37]. These are located at the centers of faceted small hillocks and were accompanied by a pair or two pairs of single atomic layer spiral steps. Figure 10 shows high resolution SFM images of nanopipes with a pair of spiral steps (Fig.10a) and with an additional single spiral step (Fig. 10b). A pair of spiral steps, each $3.1 \pm 0.8 \text{ \AA}$ high, originates at the big hole. The measured step height is consistent with the expected dimension of a single diatomic layer of GaN which is one half the length of the c-lattice parameter (2.6 \AA). Thus, the two steps form an additional complete GaN unit cell. The origin of these extra steps at the center of the hillock indicates that there is a screw dislocation in the center of the hole with a Burgers vector ($\mathbf{b} = 1/3[0003]$) equal in length to the c lattice parameter (5.2 \AA). Numerous hillocks were examined with different probe tips and similar observations were made; each has a hole with an approximately 600 \AA radius at the center. In some cases, four single steps, each $1/2 c$ high, emerged from the same hole which had a larger radius (approximately 925 \AA). This corresponds to a "giant" dislocation with Burgers vector $\mathbf{b}=2/3[0003]$. After spiraling away from the hole on the flat top of the hillock, the steps bunch together and interfere with the step emerged from other sources. In many regions, very small holes which emit single spiral steps were observed (marked with an arrow in Fig.10b). These are believed to be the mixed dislocations with a screw component of $c/2$, rather than sessile Frank partials. Since stacking faults were not observed in plan-view TEM. The apparent discrepancy between the nanopipe sizes determined from the SFM and TEM images is resolved by recognizing that the SFM image actually measures a crater on the growth surface that is always wider than the nanopipe itself. The crater can be easily observed in plan-view TEM specimens which preserve the GaN growth surface [26] and is a predicted structural component of an open-core dislocation [35].

CONCLUSIONS

Microstructure, extended defects and the growth mechanism of GaN films grown by organometallic vapor phase epitaxy on sapphire substrates using low temperature AlN (or GaN) buffer layers have been studied using a number of microscopy techniques. GaN layers grown on both a-plane and c-plane sapphire substrates using both GaN and AlN buffer layers crystallize with the same wurtzite structure and have similar microstructures. Although a number of other extended defects are often observed in the GaN films, such as stacking faults, basal plane dislocations and microtwins, the major extended defects in these films are threading dislocations and nanowires. Low angle grain boundaries are the main source of threading dislocations. These dislocations are mostly of pure edge type, running along the c-axis. The nature of these threading dislocations suggests that there should be no appreciable annihilation with the further increase of the GaN layer thickness, and the suppression of dislocations by commonly used buffer layer schemes could be more difficult. Nanowires are open-cores of screw dislocations formed under local thermodynamic equilibrium. They are about 3 - 50 nm in radii, propagate along the c axis of the film and are potentially detrimental to device applications of GaN. The nanowires are located at the centers of faceted small growth hillocks and were often accompanied by a pair or two pairs of single atomic layer spiral steps. The grain-like structure in the GaN film and the growth hillocks on the GaN free surface are related to the three dimensional growth of the buffer and the initial GaN growth. At the later stages, GaN grows by both a layer-by-layer and a spiral mechanism. It is, therefore, important to carefully optimize the buffer deposition conditions to minimize or avoid the formation of columnar structures in the GaN film.

ACKNOWLEDGMENTS

The authors acknowledge Drs. K. Doverspike, L. B. Rowland and D. K. Gaskill of Naval Research Laboratory for providing the MOVPE GaN samples used for this study. M. Shin and A. Y. Polyakov of Carnegie Mellon University for providing low temperature buffer samples used in surface studies (figure 9). W. Q. and M. S. acknowledge support under AFOSR Grant No. F29620.94.1.0392 and G.S.R. acknowledges support from the NSF under YIA Grant No. DMR-9458005.

REFERENCES

- [1] H. Morkoç, S. Strite, G. B. Gao, M. F. Lin, B. Sverdlov and M. Burns, *J. Appl. Phys.* **76**, 1363 (1994).
- [2] H. Morkoc and S.N. Mohammad, *Science*, **267**, 51 (1995).
- [3] J. I. Pankove, *Mater. Res. Soc. Symp. Proc.* **97**, 409 (1987).
- [4] S. Strite, M.E. Lin, and H. Morkoç, *Thin Solid Films*, **231**, 197 (1993).
- [5] H. Amano, N. Sawaki, I. Akasaki, and Y. Toyoda, *Appl. Phys. Letters*, **48**, 353 (1986).
- [6] H. Gotoh, T. Suga, H. Suzuki, and M. Kimata, *Japan. J. Appl. Phys.* **20**, L545 (1981).
- [7] M.J. Paisley and R.F. Davis, *J. Crystal Growth*, **127**, 136 (1993).
- [8] T. Lei, T.D. Moustakas, R.J. Graham, Y. He and S.J. Berkowitz, *J. Appl. Phys.* **71**, 4933 (1992).
- [9] S.N. Basu, T. Lei and T.D. Moustakas, *J. Mater. Res.*, **9**, 2370 (1994).
- [10] S. Strite, J. Ruan, Z. Li, N. Manning, A. Salvador, H. Chen, D.J. Smith, W.J. Choyke, H. Morkoc, *J. Vac. Sci. Technol. B*, **9**, 1924 (1991).
- [11] M.E. Lin, S. Strite, A. Agarwal, A. Salvador, G.L. Zhou, N.Teraguchi, A. Rockett and H. Morkoç, *Appl. Phys. Lett.* **62**, 702 (1993).
- [12] D.K. Wickenden, K.R. Faulkner, R. W. Brander, and B.J. Isherwood, *J. Crystal Growth*, **9**, 158 (1971).

- [13] I. Akasaki, H. Amano, Y. Koide, K. Hiramatsu, and N. Sawaki, *J. Crystal Growth*, **98**, 209 (1989).
- [14] R.C. Powell, G.A. Tomasch, Y.W. Kim, J.A. Thornton, J.E. Greene, *Mater. Res. Soc. Symp. Proc.* vol. **162**, 525 (1990).
- [15] R. C. Powell, N.-E. Lee, Y.-W. Kim and J. E. Greene, *J. Appl. Phys.*, **73**, 189 (1993).
- [16] W. Qian, M. Skowronski, M. D. Graef, K. Doverspike, L. B. Rowland and D. K. Gaskill, *Appl. Phys. Lett.*, **66**, 1252 (1995).
- [17] S. Yoshida, S. Misawa, and S. Gonda, *J. Vac. Sci. Technol. B*, **1**, 250 (1983).
- [18] J. N. Kuznia, M. A. Khan, D. T. Olson, R. Kaplan, and J.A. Freitas, Jr., *J. Appl. Phys.*, **73**, 4700 (1993).
- [19] L. B. Rowland, K. Doverspike, A. Giordana, M. Fatemi, D. K. Gaskill, M. Skowronski, and J. A. Freitas Jr., *Inst. Phys. Conf. Ser.*, **137**, 429 (1993).
- [20] K. Doverspike, L. B. Rowland, D. K. Gaskill, S. C. Binari and J. J.A. Freitas, *J. Electron. Mater.*, **24**, 269 (1995).
- [21] K. Hiramatsu, S. Itoh, H. Amano, I. Akasaki, N. Kuwano, T. Shiraishi and K. Oki, *J. Crystal Growth* **115**, 628 (1991).
- [22] T. Lei, K.F. Ludwig, and T.D. Moustakis, *J. Appl. Phys.* **74**, 4430 (1993).
- [23] Z. Liliental-Weber, H. Sohn, N. Newman and J. Washburn, *J. Vac. Sci. Technol. B* **13**, 1578 (1995).
- [24] F.A. Ponce, J.S. Major, W.E. Plano and D.F. Welch, *Appl. Phys. Lett.* **65**, 2302 (1994).
- [25] D.J. Smith, D. Chandrasekhar, B. Sverdlov, A. Botchkarev, A. Salvador and H. Morkoç, *Appl. Phys. Lett.* **67** 1830 (1995).
- [26] W. Qian, M. Skowronski, K. Doverspike, L. B. Rowland and D. K. Gaskill, *J. Crystal Growth*, **151**, 396 (1995).
- [27] D. Chandrasekhar, D.J. Smith, S. Strite, M.E. Lin and H. Morkoc, *J. Crystal Growth* **152**, 135 (1995).
- [28] S. F. Fang, K. Adomi, S. Iyer, H. Morkoç, H. Zabel, C. Choi, and N. Otsuka, *J. Appl. Phys.* **68**, R31 (1990).
- [29] K. Hiramatsu, T. Detchprohm and I. Akasaki, *Lpn. J. Appl. Phys.* **32**, (1993) 1528.
- [30] W. Qian, G.S. Rohrer, M. Skowronski, K. Doverspike, L. B. Rowland and D. K. Gaskill, *Appl. Phys. Lett.* **67**, 2284 (1995).
- [31] V. G. Bhide, *Physica*, **24**, 817 (1958).
- [32] H.M. Hobgood, D.L. Barrett, J.P. McHugh, R.C. Clarke, S. Sriram, A.A. Burk, J. Gregg, C.D. Brandt, R. H. Hopkins and W. J. Choyke, *J. Crystal Growth*, **137**, 181 (1994).
- [33] S. Takasu and S. Shimanuki, *J. Crystal Growth*, **24/25**, 641 (1974).
- [34] J. A. Powell, P. G. Neudeck, D. J. Larkin, J. W. Yang and P. Pirouz, *Inst. Phys. Conf. Ser.*, **137**, 161 (1994).
- [35] F.C. Frank, *Acta Cryst.*, **4**, 497 (1951).
- [36] J.P. Hirth and G.M. Pound, in: *Progress in Materials Science 11, Condensation and Evaporation*, Ed. B. Chalmers (Pergamon Press, New York, 1963).
- [37] X.H. Wu, D. Kopolnek, E.J. Tarsa, B. Heying, S. Keller, B.P. Keller, U.K. Mishra, S.P. DenBaars and J.S. Speck, *Appl. Phys. Lett.*, **68**, 1371 (1996).
- [38] G.S. Rohrer, J. Payne, W. Qian, M. Skowronski, K. Doverspike, L. B. Rowland, and D. K. Gaskill, *Mater. Res. Soc. Symp. Proc.* (in press).
- [39] A.A. Chernov, *Modern Crystallography III: Crystal Growth* (Springer, Berlin, 1984).